

In Silico Analysis of Pulsatile Flow Veno-Arterial Extracorporeal Membrane Oxygenation on Human Aorta Model

DHAYANANTH KANAGARAJAN^{ID,*†}, SILVER HEINSAR^{ID,‡§}, VAN THANH DAU^{ID,*}, JO P. PAULS^{ID,*}, GEOFFREY D. TANSLEY,^{*†} AND JOHN F. FRASER^{ID,‡¶}

Electrocardiogram (ECG)—synchronized pulsatile veno-arterial extracorporeal membrane oxygenation (V-A ECMO) is a recent development in extracorporeal therapy for patients with severe cardiogenic shock. Although preclinical studies have shown benefits of pulsatile flow relative to continuous ECMO flow, none have explored the effects of the timing of ECMO pulses with respect to the cardiac cycle and its possible implications on ECMO complications. This study aimed to develop a computational fluid dynamics (CFD) model of V-A ECMO in a patient-specific human aorta and evaluate the effect of ECMO timing on cardiac unloading, surplus hemodynamic energy delivery, and mixing zone position. Using direct flow measurements from cardiogenic shock patients and an ECMO device, the model revealed that maximal left ventricular (LV) unloading occurred when the ECMO pulse was in early diastole (35–40% from LV peak systolic flow). Maximum surplus hemodynamic energy transmission to aortic branches occurred at 20% from LV peak systolic flow. This indicates a trade-off between heart afterload and hemodynamic energy delivery in selecting ECMO pulse timing. The mixing zone was primarily located in the aortic arch across

timing configurations. Therefore, selecting ECMO pulse timing is crucial to maximizing the benefits of pulsatile flow in V-A ECMO treatment. ASAIO Journal 2025; 71:814–822

Key Words: pulsatile flow, computational fluid dynamics, *in silico*, V-A ECMO, mixing zone, hemodynamic energy, LV unloading

Background

Veno-arterial extracorporeal membrane oxygenation (V-A ECMO) supports refractory cardiogenic shock (CS) patients by providing temporary circulatory support or gas exchange. Veno-arterial extracorporeal membrane oxygenation is more commonly deployed using peripheral cannulation for less invasive implementation to avoid chest wall opening unless when deployed during open cardiac surgery.^{1,2} In peripheral V-A ECMO, deoxygenated blood is drained from a venous source (femoral or jugular); and oxygenated blood is returned via femoral artery, resulting in retrograde ECMO flow through the aorta instead of the native heart's antegrade flow. Rotary pumps in peripheral ECMO generate steady blood flow against systemic circulation throughout the cardiac cycle causing complications, such as left ventricular (LV) distension, suboptimal microcirculatory perfusion with end-organ failure, and blood trauma.³ In addition to this, V-A ECMO-treated patients with concomitant respiratory failure exhibit Harlequin syndrome (incidence of 13%)⁴ due to the formation of mixing zone. These complications, along with the patient's underlying disease, and CS severity, have contributed to a steady 50% mortality rate in V-A ECMO patients over the past 5 years.⁵

As ECMO is an increasingly used modality, testing for newer therapies is of particular importance. A recent advancement in ECMO technology is the addition of pulsatile flow mode offering greater hemodynamic energy transmission⁶ and other physiological benefits.⁷ Numerous studies, including *in vitro* experiments with neonatal, pediatric, and adult models demonstrate that pulsatile flow ECMO generates higher hemodynamic energy compared to nonpulsatile modes.^{8–13} Similarly, animal studies with pulsatile ECMO in acute cardiac failure¹⁴ and CS¹⁵ models show improvement in brain and renal oxygenation, LV unloading, and coronary blood flow. However, limited preclinical evidence is available on the impact of pulsatile V-A ECMO on LV unloading and end-organ microvascular perfusion.^{15,16} Therefore, this study was constructed to evaluate different pulsing timing intervals and their role in LV unloading, as well as hemodynamic energy production, which has been linked with microvascular perfusion.

In cardiovascular research, computational fluid dynamics (CFD) simulations are crucial for evaluating clinical

From the *School of Engineering and Built Environment, Griffith University, Gold Coast, Queensland, Australia; †Innovative Cardiovascular Engineering and Technology Laboratory, Critical Care Research Group, The Prince Charles Hospital, Brisbane, Queensland, Australia; ‡Faculty of Medicine, University of Queensland, Brisbane, Queensland, Australia; §Department of Intensive Care, North Estonia Medical Centre, Tallinn, Estonia; and ¶School of Medicine, Griffith University, Gold Coast, Queensland, Australia.

Submitted for consideration July 2024; accepted for publication in revised from February 2025.

Disclosure: The authors have no conflicts of interest to report.

D.K. received a scholarship from the Griffith University (Australia) for his PhD. S.H. received a scholarship from the Prince Charles Hospital Foundation (Australia) for his PhD. The Critical Care Research Group has received research funding from Xenios AG (Fresenius Medical Care), and MERA (Senko medical instrument) for ECMO research but not related to this project.

D.K., S.H., V.T.D., J.P.P., G.D.T., and J.F.F. conceptualized and designed the study. D.K. and S.H. performed the computational and experimental study, respectively. D.K., S.H., V.T.D., G.D.T., and J.F.F. performed analysis, reporting, and interpretation of data. D.K. and S.H. drafted the manuscript. All the authors assisted in the revision of manuscript. All the authors read and approved the final manuscript.

G.D.T. and J.F.F. contributed equally as co-senior authors.

Supplemental digital content is available for this article. Direct URL citations appear in the printed text, and links to the digital files are provided in the HTML and PDF versions of this article on the journal's Web site (www.asaij.org).

Correspondence: Dhayananth Kanagarajan, Innovative Cardiovascular Engineering and Technology Laboratory, Critical Care Research Group, The Prince Charles Hospital, Cheraside, Brisbane, Australia. Email: dhayaresearch001@gmail.com.

Copyright © ASAIO 2025

DOI: 10.1097/MAT.0000000000002418

interventions. Despite the possibility of utilizing lumped parameter models, the CFD approach was chosen to capture the complex and dynamic flow patterns¹⁷ observed during LV blood and ECMO blood mixing in the aorta, where flow variables—velocity and pressure vary spatially and temporally. In this study, CFD was employed to model V-A ECMO flow dynamics in a realistic patient geometry, assessing the effects of ECMO pulse timing on LV workload, hemodynamic energy transmission, mixing zone location, and aortic branch perfusion.

Methods

Human Aorta Model

A patient-specific aorta geometry developed by Stevens *et al.*¹⁸ was used to perform CFD simulations. The four-dimensional (4D)-flow magnetic resonance imaging images of a 42 year old healthy male patient were used by Stevens *et al.*¹⁸ to reconstruct the computer-aided design (CAD) model. The study was given ethics approval by relevant institutional review boards and informed consent was obtained. A schematic of the patient-specific aorta model is shown in Figure 1A. The aortic branches included in the model were brachiocephalic artery (BCA), left common carotid artery (LCCA), left subclavian artery (LSCA), celiac trunk (CT), left and right renal arteries (LRA and RRA), and left and right iliac arteries (LIA and RIA). All branches were extended by five times the diameter of the branch in length to ensure numerical convergence and more accurate results.

Grid Generation

A three-dimensional (3D) volumetric mesh with poly-hexcore elements (Figure 1, B and C) was generated using Ansys Fluent Meshing software (Ansys 2020 R2; Ansys Inc., Canonsburg). By performing mesh independence study, a mesh with 1.6 million elements and five prismatic boundary layers was selected for this work (refer to Supplemental Digital Content, <http://links.lww.com/ASAIO/B444>, for detailed information).

Numerical Modeling

Computational model and assumptions. In this study, blood was assumed to be a Newtonian fluid with a dynamic viscosity of 3.5×10^{-3} Pas, and homogenous and incompressible (density = $1,060 \text{ kg/m}^3$) to satisfy continuum hypothesis. During the cardiac cycle, the peak Reynolds number in the aorta exceeds 2,300, indicating turbulent flow. To model this, the Reynolds-averaged continuity and Navier–Stokes equations for a turbulent, incompressible, and isothermal flow were employed. The shear stress transport (SST) $k - \omega$ turbulence model^{18,19} was used to close the Reynolds form of momentum equation.

Mixing of blood from the native heart and the extracorporeal circuit is common in percutaneous V-A ECMO. In patients with lung failure, low- and high-oxygen blood streams mix inside the aorta, creating a mixing zone²⁰ where oxygen levels form a continuous spectrum between blood coming from the LV and ECMO. To model this process, a nonreactive species transport equation for oxygen was selected. The solver predicts the local mass fraction of oxygen by solving the species transport equation across the computational domain. Realistic

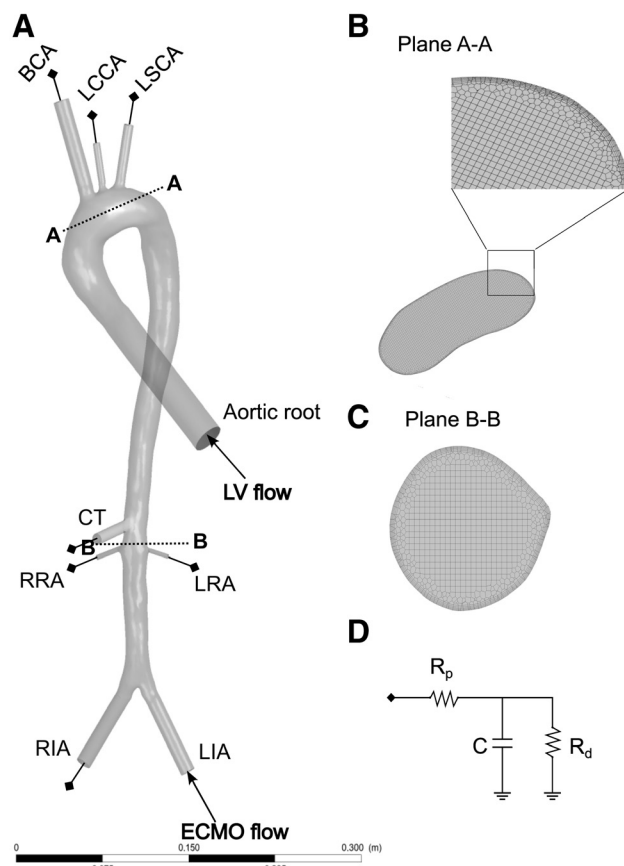


Figure 1. Schematic of the patient-specific aorta CAD model (A) with major branches employed for this study. The cross-section view of the computational domain (B, C) generated from CAD model for the planes A-A and B-B, respectively. The aortic root and LIA were provided with native heart flow modeled from a cardiogenic shock patient and ECMO device (i-Cor; Xenios AG, Heilbronn, Germany) generated flow profiles using mock circulation loop study, respectively. The remaining branches were applied with pressure values, which were calculated from solving a three-element Windkessel model. Electric analog of three-element Windkessel model (D) where R_p , C , and R_d denote proximal resistance, compliance, and distal resistance to model the arterial system downstream of respective outlets. BCA, brachiocephalic artery; CT, celiac trunk; ECMO, extracorporeal membrane oxygenation; LCCA, left common carotid artery; LIA, left iliac artery; LRA, left renal artery; LSCA, left subclavian artery; RIA, right iliac artery; RRA, right renal artery.

values of mass fraction of oxygen at aortic root and LIA, partial pressure of oxygen (pO_2) values measured using blood gas analysis were employed. These pressure values were translated to oxygen saturation data using oxyhemoglobin dissociation curve,²¹ which acts as a mass fraction of oxygen in blood. A mixture template¹⁷ was set with density, viscosity, and diffusivity values defined based on volume-weighted mixing law, mass-weighted mixing law, and constant dilute approximation (Fick's law), respectively. The diffusivity of mixture was set to $1.5 \times 10^{-9} \text{ m}^2/\text{second}$, which is the diffusivity of oxygen in human blood at 37°C .²²

Boundary conditions. To apply native heart flow as a boundary condition for the aortic root, an ensemble averaged LV flow waveform ($n = 2$) was generated from velocity time integral data of CS patients in the literature.^{23,24} Similarly, a realistic ECMO flow waveform was obtained through mock

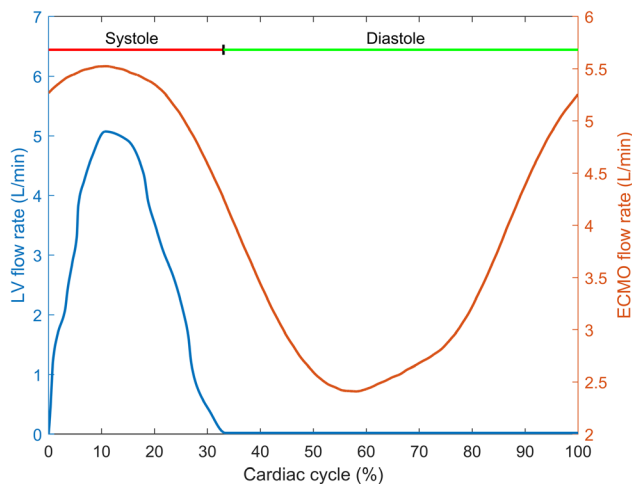


Figure 2. LV and ECMO flow waveforms with a mean cardiac output of 1 L/min and mean flow of 4 L/min, respectively. LV flow waveform was measured from cardiogenic shock patient at 80 bpm, whereas ECMO waveform generated from ECMO device (i-Cor; Xenios AG, Heilbronn, Germany) at 80 bpm. ECMO, extracorporeal membrane oxygenation; LV, left ventricular. [full color online](#)

circulatory loop experiments. These inlet waveforms—LV and ECMO, shown in Figure 2, were converted to mass flow rate and provided at aortic root and LIA as mass flow inlet boundary condition for all simulations. All outlets were provided with time-varying pressure values based on the three-element Windkessel (3EWK) model. The electric analog of this model is shown in Figure 1D. Aortic walls were modeled as rigid and impermeable and were provided with a no-slip boundary condition. For oxygen transport studies, the mass fraction of oxygen in LV and ECMO blood was defined at respective inlets. Further details on boundary conditions and numerical procedure are provided in Supplemental Digital Content, <http://links.lww.com/ASAIO/B444>.

The proposed CFD model was validated by conducting particle image velocimetry experiments. For detailed information about the construction of experimental setup and CFD model validation with experimental results, refer to Kanagarajan et al.²⁵

CFD Analysis

This study aimed to identify ECMO pulsing conditions within the cardiac cycle that minimize workload, maximize hemodynamic energy delivery, and enhance perfusion of aortic arch branches with ECMO blood. To accomplish this task, simulations were performed by varying the position of ECMO pulse peak relative to the timing of peak systolic flow of the native heart. Initially, the peak of ECMO pulse was positioned at LV peak systolic flow, and this scenario was called co-pulse mode which corresponds to 0%. Subsequently, the ECMO peak was moved every 5% of cardiac cycle and simulations were performed from 0% to 95%. The pulsing of ECMO with respect to cardiac cycle is shown in Figure 3B.

Hemodynamic analysis. To evaluate hemodynamic performance in relation to timing of the ECMO pulse during various stages of the cardiac cycle, workload of heart and hemodynamic energy—surplus hemodynamic energy (SHE) and total

hemodynamic energy (THE) were calculated in this work. The equations required for this analysis are detailed in Supplemental Digital Content, <http://links.lww.com/ASAIO/B444>.

Mixing zone analysis. Mixing zone is the region where the ECMO blood and LV blood collide. In patients with lung failure, residual cardiac blood flow can become hypoxic, causing the upper body to receive blood with lower oxygen content than the lower body, resulting in differential hypoxia. In the upper body, the brain is the most critical organ requiring a constant supply of oxygenated blood to avoid cerebral hypoxia. For adequate brain function, blood pO_2 must be at least 40 mm Hg,²⁶ corresponding to an SpO_2 of 71%, which was used as the threshold in this study. To identify this point, several equidistant planes perpendicular to flow direction were created from the aortic root to the LIA branch excluding flow extensions, using the *point and normal* method in Ansys CFD Post. The average mass fraction of oxygen was calculated for each plane to locate the brain threshold point. Additionally, mass fraction of oxygen in blood leaving each aortic outlet was analyzed to substantiate the mixing zone's position.

Results

Left Ventricular Workload

Figure 3A illustrates changes in cardiac workload with ECMO pulse timing during a cardiac cycle. Workload drops as the ECMO pulse peak moves away from LV peak systolic flow, reaching a minimum of 0.24 W at 35–40% before rising to a maximum of 0.27 W at 90%. The effect of retrograde pulsatile flow ECMO on the pressure waveform measured at the level of aortic root is shown in Figure 3, C and D (presented in two graphs to reduce complexity). Peak systolic pressure decreases as the ECMO pulse position moves from 0–35% and increases again from 40% to 90%, while diastolic pressure follows the opposite trend. Throughout the study, systolic pressure was closest to 120 mm Hg at ECMO pulse position between 5% and 10% and 65% and 75%, while diastolic pressure remained higher than 80 mm Hg for all positions of the ECMO pulse. A second pressure peak, corresponding to ECMO pulsation was visible in pressure waveforms when the ECMO pulse was positioned between 15% and 65%. For other cases, the second peak is absent due to the overlap of ECMO pulse and LV systolic contraction.

Hemodynamic Energy

The hemodynamic energy delivered to organs is quantified by calculating THE and SHE for each ECMO pulse timing. Figure 4A shows the sum of individual THE calculated across aortic branches. Maximum THE occurs at ECMO pulse position of 5%, while the minimum occurs at 55%. For SHE (Figure 4B), maximum SHE of 8,039 J/m³ was observed at 20% and a minimum of 1,160 J/m³ was observed at 60%. Table 1 shows the maximum SHE at 20% for all branches except LSCA, which peaks at 15%. Minimum SHE delivery occurs at 60% for BCA and LSCA branches and at 65% for other branches (LCCA, CT, LRA, RRA) in the aorta.

The combined behavior of cardiac workload and surplus hemodynamic energy for different ECMO pulse timings is shown in Figure 5A. Maximum SHE delivery occurs at 20%

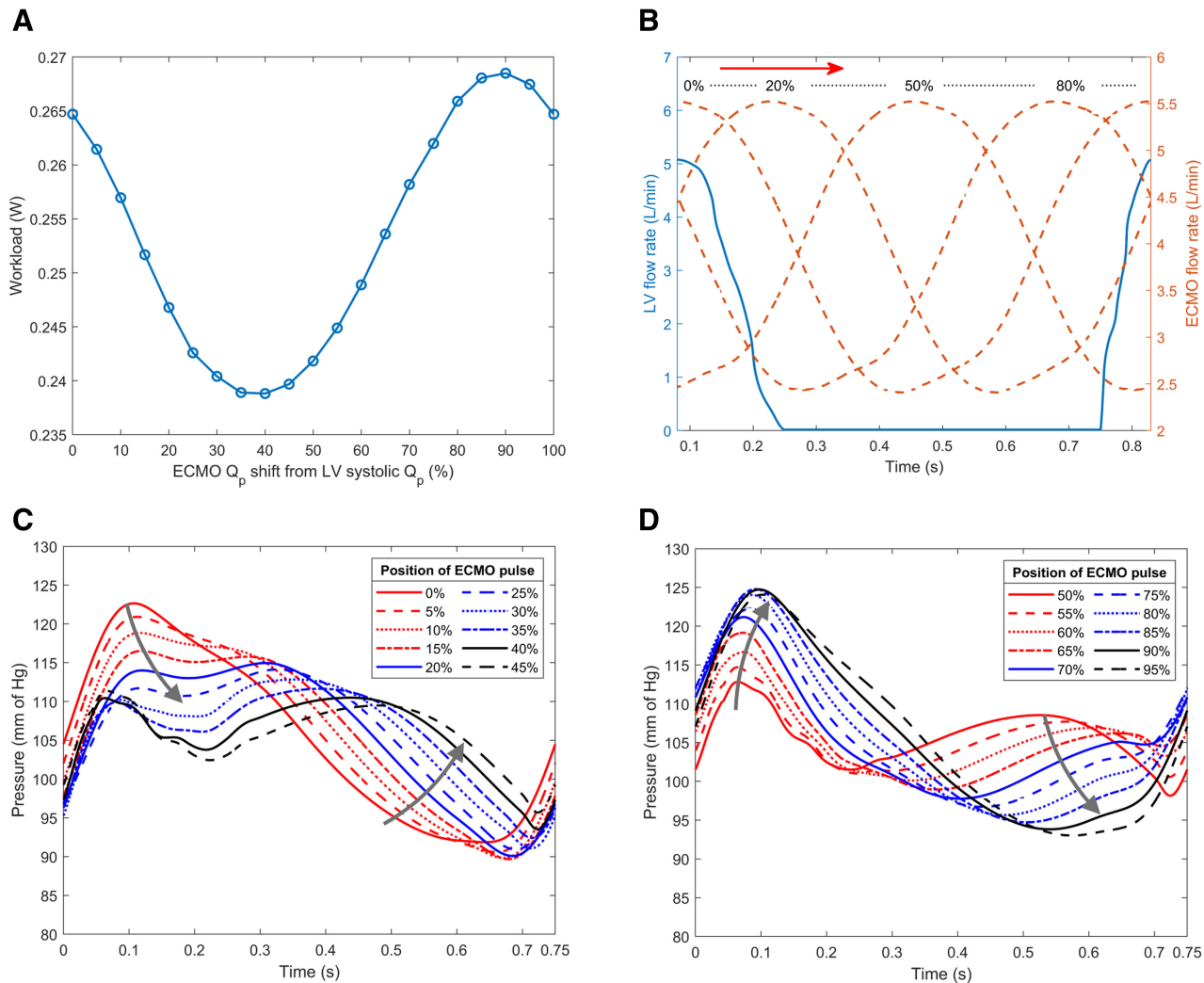


Figure 3. **A:** Variation in afterload of heart under pulsatile flow V-A ECMO support. The ECMO pulse position is varied by shifting the peak of ECMO pulse with respect to LV peak systolic flow. Timing of ECMO pulse is expressed as percentage of cardiac cycle. **B:** Arrangement of ECMO pulse with respect to the cardiac cycle of the native heart, where position of both pulse peaks which are in phase with each other, is selected as starting point (denoted by 0%). The ECMO pulse peak is shifted by 5% of cardiac cycle starting from 0% to 95%. Red arrow in subplot (B) indicates the direction of ECMO pulse movement with respect to native heart flow. **C, D:** The pressure trends measured at the aortic root with increased displacement of the ECMO pulse with respect to the cardiac cycle. The legend shows the movement of the ECMO pulse from the peak systolic flow of native heart. The arrow marks denote the increasing and decreasing trend of systolic and diastolic pressure in a cardiac cycle. ECMO, extracorporeal membrane oxygenation; LV, left ventricular; Q_p , peak flow. [full color online](#)

from LV peak systolic flow, whereas minimum workload occurs at 35–40%. Figure 5B shows arterial pressure waveform measured at all aortic branches for ECMO pulse at 20%. Supra aortic branches (BCA, LCCA, LSCA) exhibit dual peaks, whereas branches in the abdominal aorta show single peak during cardiac cycle. Renal arteries had lower systolic and diastolic pressures than other arteries. Pressure waveforms of BCA and RIA branch were measured for ECMO pulse position of 0%, 20%, 40%, 60%, and 80% (Figure 5, C and D). Brachiocephalic artery exhibited dual peaks in pressure waveforms for ECMO pulse position 20%, 40%, and 60%. Peak pressure values observed for ECMO pulse locations 0% and 80% were higher than those of other locations. For the RIA branch, dual peaks appeared for ECMO pulse positions at 40% and 60%. Dual-peak waveforms lower peak pressures compared to single-peak waveforms in both branches.

Mixing Zones

The location of mixing zone during various key positions in a cardiac cycle for different ECMO pulse movements is shown in Figure 6, A and B. For all ECMO pulse positions, the mixing zone was located between LCCA and LSCA branches. The visualization of mixing zone in the aortic arch is highlighted in Figure 6C. Oxygen saturation of blood leaving each branch in the aorta model was measured and shown in Figure 6, D and E. Brachiocephalic artery and LCCA branches received blood with oxygen saturation values close to 60% for different ECMO pulse timings. However, blood leaving LSCA branch in aortic arch exhibits oxygen saturation close to 90%. Other abdominal aorta branches such as CT, LRA, RRA, and RIA received blood with an oxygen saturation of 100%. Except for BCA and LSCA, all other branches received blood with oxygen saturations greater than 71%.

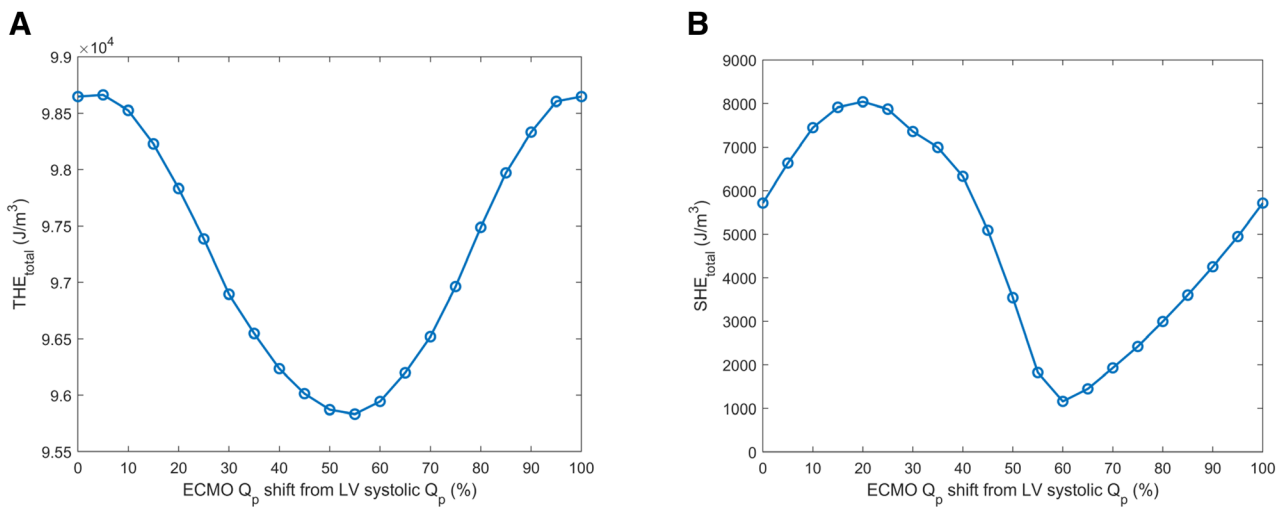


Figure 4. Effect of different ECMO pulse position on THE and SHE delivered to various branches in the aorta. THE_{total} represents sum of THE of all branches (A) and SHE_{total} represents sum of SHE of all branches (B). ECMO, extracorporeal membrane oxygenation; Q_p, peak flow; SHE, surplus hemodynamic energy; THE, total hemodynamic energy.

[full color online](#)

Table 1. Aortic Branches Exhibiting Maximum and Minimum SHE Delivery

Branch	ECMO Pulse Position for Max SHE Delivery	ECMO Pulse Position for Min SHE Delivery
BCA	20%	60%
LCCA	20%	65%
LSCA	15%	60%
CT	20%	65%
LRA	20%	65%
RRA	20%	65%
RIA	20%	70%

BCA, brachiocephalic artery; CT, celiac trunk; ECMO, extracorporeal membrane oxygenation; LCCA, left common carotid artery; LIA, left iliac artery; LRA, left renal artery; LSCA, left subclavian artery; max, maximum; min, minimum; RIA, right iliac artery; RRA, right renal artery; SHE, surplus hemodynamic energy.

Discussion

Synchronized pulsatile V-A ECMO is a recent development in ECMO technology potentially beneficial for patients with CS. Our recent systematic review²⁷ found that most preclinical studies on pulsatile flow in V-A ECMO focus on hemodynamic energy production, which was higher in pulsatile flow compared to continuous flow. This study evaluates the effect of ECMO pulse timing with the cardiac cycle on cardiac unloading, hemodynamic energy delivery, and dynamics of mixing zones, critical for patient recovery and minimizing ECMO-related complications.

Optimal Timing for Left Ventricular Unloading

Left ventricular distension²⁸ is a serious complication in V-A ECMO patients with acute cardiac failure, caused by low LV contractility, high afterload, impaired LV ejection, and an imbalanced myocardial oxygen supply-demand ratio. Several mechanisms can contribute to this increased afterload, including increased systemic vascular resistance and retrograde ECMO circulation from continuous propulsion of blood by peripherally inserted ECMO device. Our study highlights that pulsatile ECMO flow, timed adequately, reduces afterload from ECMO circulation. Positioning the ECMO pulse at 35–40% of LV peak systolic flow corresponds to 46% of

the cardiac cycle, indicating pulse delivery during diastole. Maximum LV unloading (minimum workload) occurs in early diastole, not late diastole, where ECMO pulse overlaps with aortic valve opening. This overlap may be due to the time required for the pulse wave to travel from the ECMO device to the heart. Additionally, the sine-wave shape of the ECMO pulse generated by the diagonal pump reduces workload by smoothing flow transitions (LV flow deceleration and ECMO flow acceleration). These factors lower systolic pressure at the aortic root, minimizing workload at 35–40% ECMO pulse timing (Figure 3A). Conversely, ECMO pulses delivered closer to peak systole increase arterial pressure at the aortic root (Figure 3, C and D) due to LV and ECMO flow collision, causing localized pressure spikes. Delaying ECMO pulse timing can mitigate these effects.

Maximizing Hemodynamic Energy Transmission

The purpose of peripheral V-A ECMO is to deliver oxygenated blood with sufficient hemodynamic energy to perfuse organs, previously delivered by the healthy native heart. Hemodynamic energy in the aorta, calculated using energy equivalent pressure defined by Shepard et al.,⁶ peaks when LV peak systolic flow aligns with the ECMO pulse at 5% (Figure 4A). This collision increases systolic arterial pressure and flow, beneficial for hemodynamic energy but potentially

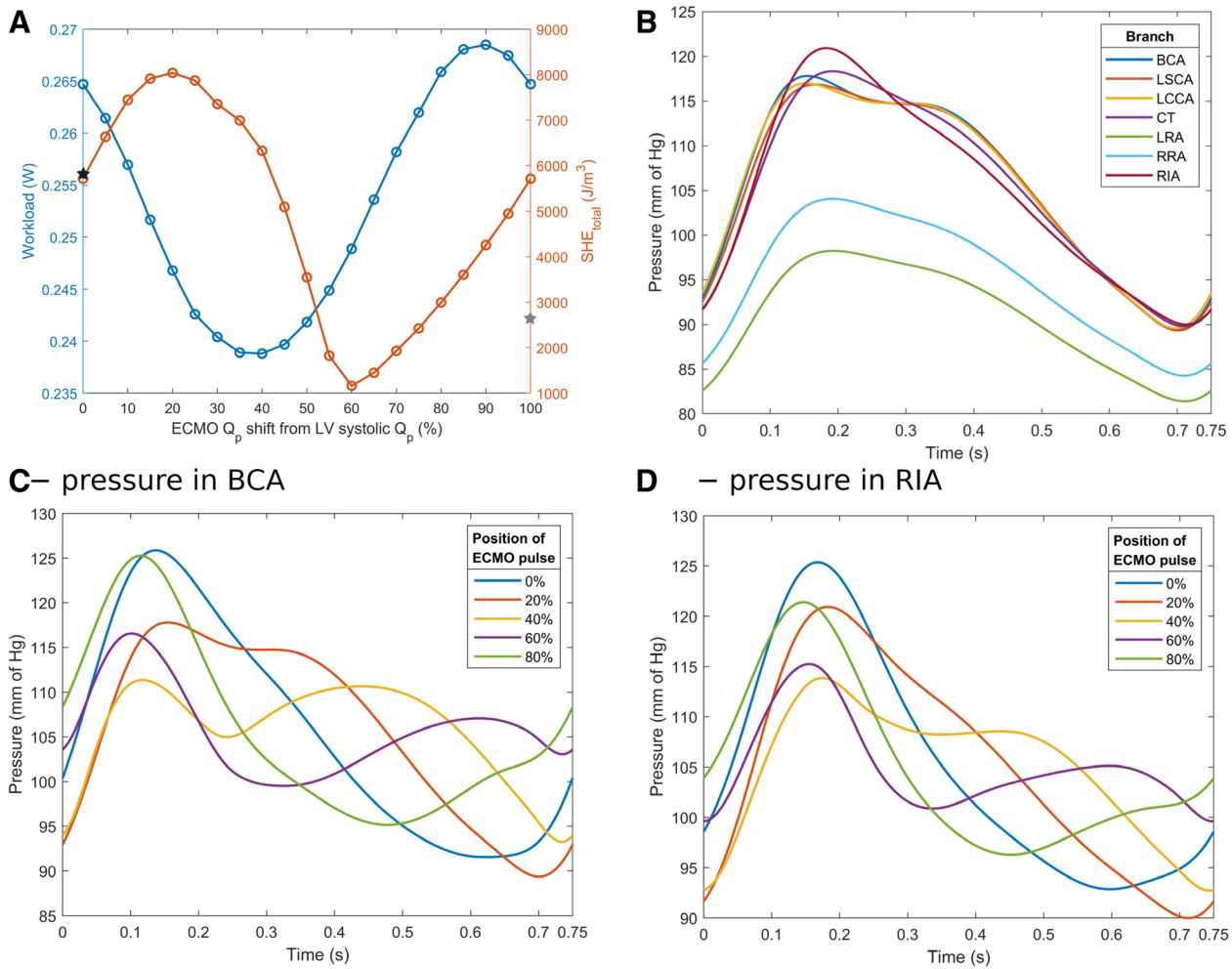


Figure 5. A: Comparison of workload of heart and SHE delivered to various aortic branches for different position of ECMO pulse in a cardiac cycle. Black and gray filled star symbols correspond to workload and SHE for continuous flow V-A ECMO. **B:** Pressure waveform measured at all outlet branches when ECMO pulse position at 20% of cardiac cycle from peak systolic flow, chosen because of high energy transfer with low cardiac workload. Variation of pressure waveform in BCA (**C**) and RIA (**D**) branches for ECMO pulse position of 0%, 20%, 40%, 60%, and 80%. BCA, brachiocephalic artery; CT, celiac trunk; ECMO, extracorporeal membrane oxygenation; LCCA, left common carotid artery; LIA, left iliac artery; LRA, left renal artery; LSCA, left subclavian artery; Q_p , peak flow; RIA, right iliac artery; RRA, right renal artery.

[full color online](#)

harmful due to increased LV afterload. From the hemodynamic energy standpoint, it will be beneficial. However, when assessing from an afterload standpoint, this may overload an already weakened left ventricle. Thus, there is a trade-off between hemodynamic energy and LV distension and worsening myocardial ischemia. To evaluate the hemodynamic energy contributed by the pulsatile flow, the SHE is calculated, quantifying the benefit of pulsatile flow to keep capillary beds in microcirculation open and maintain an aerobic cellular metabolism in tissues.²⁹ In a severe CS animal model, our group (Heinsar *et al.*³⁰) showed that employing pulsatile flow in V-A ECMO configuration improves microcirculation with greater SHE values than continuous flow. Maxima and minima for SHE occurred for ECMO pulse positions of 20% and 60% from LV peak systolic flow, respectively (Figure 4B). At 20%, the ECMO pulse wave occurs late enough and avoids colliding with the native heart's pulse, maximizing SHE, as confirmed by timings at individual aortic branches (Table 1).

Trade-Off Between Cardiac Unloading and Hemodynamic Energy

This computational study on pulsatile V-A ECMO has demonstrated that timing the ECMO pulse relative to native heart cycle is crucial for benefits like cardiac unloading and surplus hemodynamic energy delivery. However, a trade-off between minimizing ventricular workload (optimal at 35–40%) and maximizing SHE delivery (optimal at ~20% from LV peak systolic flow). Notably, at around 20–30% of LV peak systolic flow, a balance of low workload and high SHE delivery can be achieved (Figure 5A). Based on the clinical scenario and dominating pathology (cardiac distension *versus* microvascular collapse), ECMO pulse timing could be customized to the patient's condition. For imminent aortic valve closure, ECMO pulse could be timed to 40% to maximize unloading while still delivering sufficient SHE to the microcirculation. For cases prioritizing microvascular perfusion, such as cardiac arrest survivors, timing at 20%, maximizes SHE levels. Timing outside the 20–40% range may reduce microcirculatory benefits

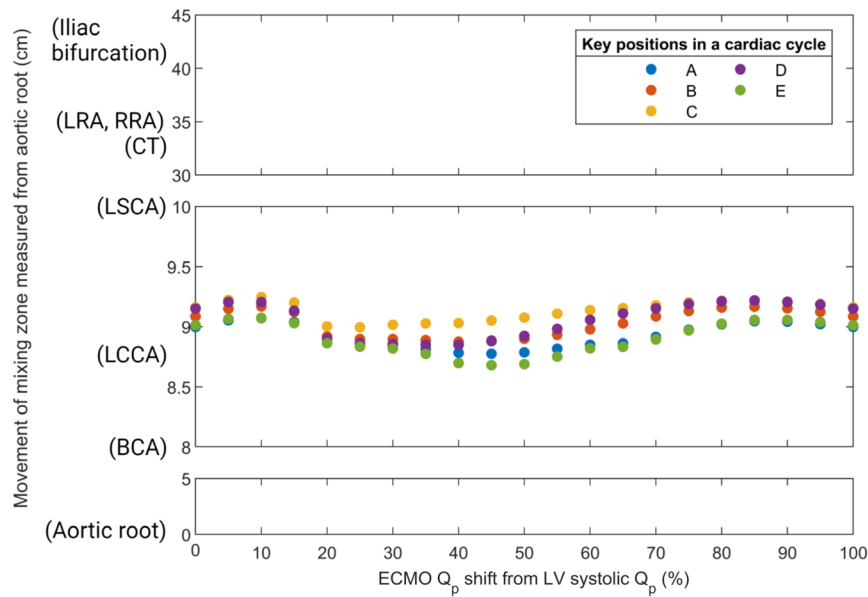
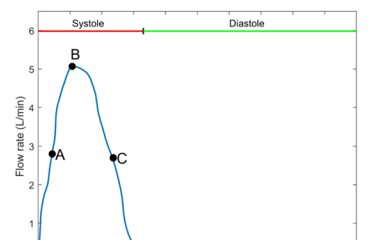
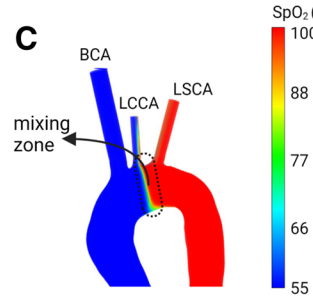
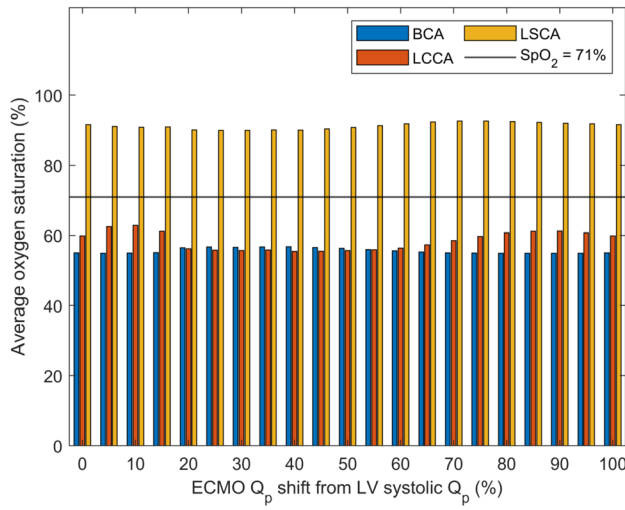
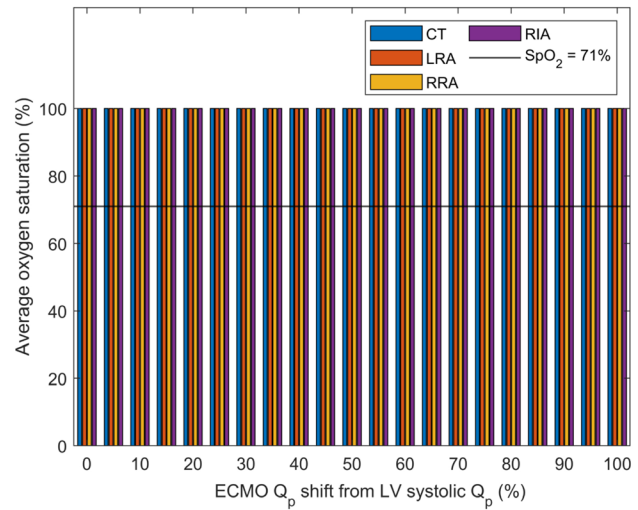
A**B****C****D****E**

Figure 6. **A:** Comparison of mixing zone movement over various key positions in a cardiac cycle for different ECMO pulse timing with ECMO flow contributing 80% of total organ perfusion. The ordinate denotes mixing zone movement in centimeters (cm) measured from aortic root and corresponding branch name is mentioned in parentheses. **B:** The key positions in a cardiac cycle employed for measuring mixing zone in panel (A). **C:** The volume rendering of oxygen saturation in human aorta during peak systolic flow for the ECMO pulse position of 0%. **D, E:** The oxygen saturation of blood leaving aortic branches. Except BCA and LCCA, remaining branches received enough oxygen during pulsatile V-A ECMO support. The oxygen saturation of 71% is selected as minimum oxygen requirement shown using black line. BCA, brachiocephalic artery; CT, celiac trunk; LCCA, left common carotid artery; LIA, left iliac artery; RIA, right iliac artery; RLA, left renal artery; LSCA, left subclavian artery; Q_p, peak flow; RRA, right renal artery; V-A ECMO, veno-arterial extracorporeal membrane oxygenation. full color online

or increase cardiac workload, potentially raising LV afterload when compared to continuous flow.

In clinical settings, a key challenge is choosing an optimal delay trigger for ECMO pulse to maximize pulsatile V-A ECMO benefits. Ideally, the ECMO device monitors would display real-time SHE values and cardiac workload, requiring constant measurement of SHE in arterial branches alongside pressure-volume loops. Whilst this is currently

unrealistic, Figure 5, C and D suggest an alternative: clinicians could match their observed arterial waveforms (from radial or femoral arteries, depending on pressure cannula placement) with the timing percentages in this study. Further *in vivo* validation is required to confirm these waveforms. This approach could enable personalized ECG-synchronized pulsatile V-A ECMO therapy with standard ICU monitoring for the critically ill.

Mixing Zone Dynamics

Differential hypoxemia is another serious complication in patients with peripheral V-A ECMO with concomitant respiratory failure. In a large animal model of cardiorespiratory failure supported by continuous flow V-A ECMO, our group (Rozencwajg et al.³¹) showed that higher flow rates improve cerebral oxygenation and reduce brain injury when compared to lower flow rates but increase LV afterload. Present work modeled the mixing zone position in pulsatile V-A ECMO and reported brain oxygen saturation levels. Blood leaving LV was assumed to be severely hypoxic (SpO_2 of 55%) due to lung failure, with the gas blender FiO_2 set to 1.0. Previous *in silico* studies^{18,32,33} modeled the mixing zone as a region where LV blood and ECMO blood mix equally, regardless of oxygen levels. Although mixing can be localized, oxygen delivery to major aortic branches remains hypothetical. This study modeled the mixing zone with an SpO_2 of 71%—the minimum required for brain function. For all ECMO pulse timings, the mixing zone was between LCCA and LSCA when ECMO flow contributed 80% (4 L/min) of total organ perfusion (Figure 6A). Diastolic pulsing from the ECMO device caused mixing zone shifts during acceleration and deceleration phases of the ECMO flow. Therefore, shifting of mixing zone during the cardiac cycle is related to pulsatile amplitude settings in the ECMO machine. Oxygen saturations entering individual branches confirmed the location of mixing zone. Except for BCA and LCCA, all the remaining branches were perfused with oxygenated blood from ECMO device, while the aortic root, ascending aorta, and part of aortic arch received LV blood. This may result in cerebral and coronary hypoxia for patient with severe lung failure, not fully addressed, by pulsatile flow in V-A ECMO circuits. However, animal studies^{15,30,34} have reported reduced cerebral and coronary hypoxia during pulsatile flow compared to continuous flow V-A ECMO.

Limitations

Although this study enhances understanding of ECMO pulse timing on cardiac unloading and hemodynamic energy delivery, it has limitations. Aortic walls were modeled as non-compliant, whereas human aortas are compliant with patient-specific variations. A fluid-structure interaction study should be performed in future to capture the influence of wall compliance. This study employs flow waveforms directly measured from the heart. However, to reduce the model's complexity Frank-Starling mechanism and left and right ventricular functions were excluded. Future work will include these factors. Constant oxygen partial pressure values were used to model ECMO and LV blood mixing, but future studies will account for varying partial pressures. Reynolds numbers inside aorta (1,236–2,827) indicated transitional or relaminarizing flow in parts of the cardiac cycle, which is challenging to model with a high degree of accuracy. An SST model with high tolerance for relaminarizing flows and low turbulence was used, with laminar flow model showing less than or equal to 5% differences. The iliac artery boundary condition was based on flow profiles measured post-oxygenator, but cannula-specific factors (eg, insertion location, length, and tip design) affecting flow delivery were not modeled. Future work should include cannula modeling within human aorta. The present work

considered only one heart rate, representing CS patients, but heart rate variations affecting pulsing ability and heart systole-to-diastole ratios require further exploration. Different pulsatile ECMO devices might have different implications on unloading and energy generation. This study used a sine wave from the i-Cor® device (Xenios AG, Heilbronn, Germany), the predominantly studied pulsatile ECMO machine. Future studies should look at different pulsatile waveforms. This study was based on a single healthy-patient-derived aorta model, which may differ from diseased patient anatomy. However, ECMO patients are often also otherwise healthy,³⁵ supporting the generalizability of findings with individual adjustments.

Conclusions

This study demonstrates the potential clinical benefits of synchronized pulsatile V-A ECMO for severe heart failure patients. Proper ECMO pulse timing could reduce LV distension and microcirculatory dysfunction and be tailored to individual patient conditions. Pressure waveforms of brachial and femoral arteries could guide clinicians in adjusting ECMO device delay triggers. However, differential hypoxia was not fully addressed by any pulsatile ECMO setting. Rigorous *in vitro* studies and animal trials are needed to validate these findings and ensure effective clinical translation.

Acknowledgments

This research was supported by the Griffith University Gowonda HPC Cluster. Figure 2, A and B, Supplemental Digital Content, <http://links.lww.com/ASAIO/B444>, were created using Biorender.com.

References

- Mariscalco G, Salsano A, Fiore A, et al; PC-ECMO Group: Peripheral versus central extracorporeal membrane oxygenation for postcardiotomy shock: Multicenter registry, systematic review, and meta-analysis. *J Thorac Cardiovasc Surg* 160: 1207–1216.e44, 2020.
- Pavlushkov E, Berman M, Valchanov K: Cannulation techniques for extracorporeal life support. *Ann Transl Med* 5: 70, 2017.
- Chommeloux J, Montero S, Franchineau G, et al: Microcirculation evolution in patients on venoarterial extracorporeal membrane oxygenation for refractory cardiogenic shock. *Crit Care Med* 48: e9–e17, 2020.
- Contento C, Battisti A, Agrò B, et al: A novel veno-arteriovenous extracorporeal membrane oxygenation with double pump for the treatment of Harlequin syndrome. *Perfusion* 35(1_suppl): 65–72, 2020.
- (ELSO) ELSO: ELSO Live Registry Dashboard of ECMO Patient Data. Available at: <https://www.elso.org/registry/elсолiveregistrydashboard.aspx>. Accessed 28 January, 2023.
- Shepard RB, Simpson DC, Sharp JF: Energy equivalent pressure. *Arch Surg* 93: 730–740, 1966.
- Wilkins H, Regelson W, Hoffmeister FS: The physiologic importance of pulsatile blood flow. *N Engl J Med* 267: 443–446, 1962.
- Adedayo P, Wang S, Kunselman AR, Undar A: Impact of pulsatile flow settings on hemodynamic energy levels using the novel diagonal Medos DP3 pump in a simulated pediatric extracorporeal life support system. *World J Pediatr Congen Heart Surg* 5: 440–448, 2014.
- Evenson A, Wang S, Kunselman AR, Undar A: Use of a novel diagonal pump in an *in vitro* neonatal pulsatile extracorporeal life support circuit. *Artif Organs* 38: E1–E9, 2014.
- Krawiec C, Wang S, Kunselman AR, Undar A: Impact of pulsatile flow on hemodynamic energy in a Medos Deltastream DP3

- pediatric extracorporeal life support system. *Artif Organs* 38: 19–27, 2014.
11. Wang S, Kunselman AR, Uendar A: Novel pulsatile diagonal pump for pediatric extracorporeal life support system. *Artif Organs* 37: 37–47, 2013.
 12. Wang S, Moroi M, Brehm CE, Kunselman AR, Undar A: In vitro hemodynamic evaluation of an adult pulsatile extracorporeal membrane oxygenation system. *Artif Organs* 42: E234–E245, 2018.
 13. Wolfe R, Strother A, Wang S, Kunselman AR, Ündar A: Impact of pulsatility and flow rates on hemodynamic energy transmission in an adult extracorporeal life support system. *Artif Organs* 39: E127–E137, 2015.
 14. Itoh H, Ichiba S, Ujike Y, et al: Effect of the pulsatile extracorporeal membrane oxygenation on hemodynamic energy and systemic microcirculation in a piglet model of acute cardiac failure. *Artif Organs* 40: 19–26, 2016.
 15. Ostadal P, Mlcek M, Gorhan H, et al: Electrocardiogram-synchronized pulsatile extracorporeal life support preserves left ventricular function and coronary flow in a porcine model of cardiogenic shock. *PLoS One* 13: e0196321–e0196321, 2018.
 16. Li G, Zhu S, Zeng J, et al: Arterial pulsatility augments microcirculatory perfusion and maintains the endothelial integrity during extracorporeal membrane oxygenation via hsa_circ_0007367 upregulation in a Canine model with cardiac arrest. *Oxid Med Cell Longev* 2022: 1630918, 2022.
 17. Seetharaman A, Keramati H, Ramanathan K, et al: Vortex dynamics of veno-arterial extracorporeal circulation: A computational fluid dynamics study. *Phys Fluids* 33: 061908, 2021.
 18. Stevens MC, Callaghan FM, Forrest P, Bannon PG, Grieve SM: Flow mixing during peripheral veno-arterial extracorporeal membrane oxygenation—A simulation study. *J Biomech* 55: 64–70, 2017.
 19. Zhang Q, Gao B, Shi Y, Yu C: The hemodynamic comparative study between pulsatile and non-pulsatile VA ECMO: A primary numerical study. *Computer Modeling Eng Sci* 116: 247–262, 2018.
 20. Winiszewski H, Guinot P-G, Schmidt M, et al: Optimizing PO₂ during peripheral veno-arterial ECMO: A narrative review. *Crit Care* 26: 226, 2022.
 21. Chambers D, Huang C, Matthews G: *Basic Physiology for Anaesthetists*, 2 ed. Cambridge University Press, 2019.
 22. Goldstick TK, Ciuryla VT, Zuckerman L: Diffusion of oxygen in plasma and blood. *Adv Exp Med Biol* 75: 183–190, 1976.
 23. Mohammad A, Karamat S, Majeed Y, Silvet H, Abramov D: Echo-based hemodynamics to help guide care in cardiogenic shock: A review. *Curr Cardiovasc Imaging Rep* 15: 57–67, 2022.
 24. Théry G, Gascon V, Fraile V, Ochagavia A, Hamzaoui O: How to use echocardiography to manage patients with shock? *Med Intensiva* 48: 220–230, 2024.
 25. Kanagarajan D: *Computational Fluid Dynamics Study of Mixing Zones in Extracorporeal Membrane Oxygenation Circuits to Improve Outcomes*. Gold Coast, Queensland, Australia, School of Eng & Built Env, Griffith University, 2024.
 26. Hadanny A, Efrati S: Oxygen—A limiting factor for brain recovery. *Crit Care* 19: 307, 2015.
 27. Kanagarajan D, Heinsar S, Gandini L, et al: Preclinical studies on pulsatile veno-arterial extracorporeal membrane oxygenation: A systematic review. *ASAIO J* 69: e167–e180, 2023.
 28. Rajagopal K: Left ventricular distension in veno-arterial extracorporeal membrane oxygenation: From mechanics to therapies. *ASAIO J* 65: 1–10, 2019.
 29. Ji B, Undar A: Comparison of perfusion modes on microcirculation during acute and chronic cardiac support: Is there a difference? *Perfusion* 22: 115–119, 2007.
 30. Heinsar S, Sato K, Obonyo N, et al: Improved microcirculation with pulsatile veno-arterial ECMO: An ovine model of cardiogenic shock. *Am J Respir Crit Care Med* 209: 1396–1399, 2024.
 31. Rozencwajg S, Heinsar S, Wildi K, et al: Effect of flow change on brain injury during an experimental model of differential hypoxaemia in cardiogenic shock supported by extracorporeal membrane oxygenation. *Sci Rep* 13: 2023, 4002.
 32. Nezami FR, Khodaei F, Edelman ER, Keller SP: A computational fluid dynamics study of the extracorporeal membrane oxygenation-failing heart circulation. *ASAIO J* 67: 276–283, 2021.
 33. Nezami FR, Ramezanpour M, Khodaei F, Goffer E, Edelman ER, Keller SP: Simulation of fluid-structure interaction in extracorporeal membrane oxygenation circulatory support systems. *J Cardiovasc Transl Res* 15: 249–257, 2022.
 34. Cremers B, Link A, Werner C, et al: Pulsatile venoarterial perfusion using a novel synchronized cardiac assist device augments coronary artery blood flow during ventricular fibrillation. *Artif Organs* 39: 77–82, 2015.
 35. Alnahhal KI, Majumdar M, Irshad A, Kapur N, Kumar S, Salehi P: Peripheral artery disease and extracorporeal membrane oxygenation: Examining a high-risk cohort over time. *Vascular* 32: 867–873, 2024.